DOI: 10.26599/FSHW.2026.9250999

Contents lists available at SciOpen

Food Science and Human Wellness

journal homepage: https://www.sciopen.com/journal/2097-0765

China Food Publishing Co.

Multi-omics Insights into the Mitigation of Diet-induced Obesity by Dendrobium officinale Polysaccharides via Gut-Adipose Tissue Axis Modulation of Lipid Droplets

Xiajialong Li, Shenji Yang, Xiaojun Huang, Jing Feng, Zhikang Cao, Peng Chen, Shuigen Bian, Zhipeng Li*, Mingyong Xie*

State Key Laboratory of Food Science and Resources, China-Canada Joint Lab of Food Science and Technology (Nanchang), Nanchang University, Nanchang 330047, China

ABSTRACT: The rising prevalence of overweight and obesity poses a significant threat to life quality. Although *Dendrobium officinale* polysaccharide (DOP) has demonstrated various health benefits, its effects on obesity and the underlying mechanisms remain to be fully elucidated. This study, using a high-fat diet-induced obesity (DIO) mouse model, shows that DOP significantly alleviates DIO by suppressing lipid droplet (LD) expansion and downregulating LD-associated genes, including PLIN2 and PLIN3, in white adipose tissue (WAT). These genes positively correlate with metabolic parameters including body weight gain, adiposity, and glucose intolerance. A meta-analysis further reveals that PLIN2 and PLIN3 are consistently upregulated in the adipose tissues of both obese mice and humans, underscoring their clinical relevance. Transcriptomic analysis indicates that DOP potentially activates the Wnt signaling pathway in WAT, thereby suppressing lipid synthesis and storage and inhibiting adipocyte differentiation. Metagenomic analysis demonstrates that DOP reverses obesity-associated gut microbiota dysbiosis by downregulating bacteria positively associated with LD formation and obesity phenotypes, while upregulating bacteria negatively associated with these traits. Notably, a data-driven analysis identified *Bifidobacterium pseudolongum* and *B. choerinum* as potential key mediators of DOP's effects. Untargeted metabolomics reveals that DOP reshapes serum metabolite profiles, particularly upregulating acylcarnitines, which negatively correlate with LD formation and metabolic parameters. A multi-omics covariance network integrating gut microbiota, serum metabolites, WAT gene expression, and metabolic phenotypes suggests that DOP modulates lipid metabolism possibly through gut microbiota and metabolites, thereby improving obesity-related traits. In conclusion, this multi-omics study is the first to suggest that DOP may promote the Wnt signaling pathway and inhibit LD expansion through the gut-adipose axis, thereby mitigating the onset of DIO.

Keywords: *Dendrobium officinale* polysaccharides, obesity, white adipose tissue, lipid droplet, Wnt signaling, gut microbiome, multi-omics

1. Introduction

As living standards improve, overweight and obesity have become global health issues. According to the World Health Organization, in 2022 43% of adults aged 18 years and over were overweight and 16% were

***Corresponding author**
Zhipeng Li email: zhipengli@ncu.edu.cn
Mingyong Xie email: myxie@ncu.edu.cn

Received 11 June 2025
Received in revised from 2 August 2025
Accepted 7 November 2025

living with obesity[1]. Obesity is a major risk factor for metabolic diseases including type 2 diabetes (T2D) and fatty liver disease[2]. *Dendrobium officinale* is widely used as both a food ingredient and herbal medicine in China, with *Dendrobium officinale* polysaccharide (DOP) being one of its primary bioactive components[3]. Studies have shown that DOP can improve diabetes induced by a high-fat diet (HFD) combined with streptozotocin[4]. However, systematic evaluations of its effects on obesity are lacking, and the molecular biological mechanisms of its anti-obesity effects remain unclear.

Obesity is primarily characterized by the excessive accumulation of fat in the body. The gut microbiota plays a crucial regulatory role in lipid metabolism, including biological processes such as lipid synthesis and thermogenesis[5, 6]. It has been well-established that germ-free mice or mice treated with antibiotics exhibit reduced weight gain and fat mass increase when fed an obesogenic diet[7, 8]. As a major substrate for gut microbiota, dietary fiber is essential for modulating its composition and activity[9]. Therefore, DOP may exert its effects on lipid metabolism in adipose tissue by influencing the gut microbiota.

White adipose tissue (WAT) is one of the organs/tissues most significantly affected in diet-induced obesity (DIO)[10]. Lipid droplets (LDs), organelles surrounded by a monolayer phospholipid membrane, function beyond lipid storage within cells and play vital roles in many biological processes, including energy storage, lipid metabolism, and cell signaling[11]. Therefore, a deeper understanding of the formation and regulatory mechanisms of LDs is crucial for preventing metabolic diseases such as obesity, diabetes, and fatty liver.

Perilipins are a family of proteins that coat the surface of LDs and play critical roles in LD formation and degradation[12]. Overexpression of PLIN2 has been shown to promote LD accumulation in COS-7 and fibroblast cells[13, 14], while knockout of PLIN2 significantly improves DIO, WAT inflammation, and fatty liver[15]. Studies have found that a Pro251 mutation in PLIN2 is strongly associated with enhanced insulin sensitivity in obese individuals[16]. In addition, PLIN3 also regulates LD dynamics. Reduced PLIN3 expression decreases triglyceride levels in THP-1 macrophages, whereas PLIN3 overexpression increases triglyceride accumulation[17]. Furthermore, in PLIN2-deficient cells, PLIN3 is compensatorily upregulated[18, 19]. These findings suggest that overexpression of PLIN2 and PLIN3 may promote LD formation and lipid over-accumulation, while suppressing their expression could help prevent obesity.

Dietary components often have complex structures and may interact through multiple mechanisms within the body, ultimately influencing phenotypes. Systems biology approaches, utilizing multi-omics techniques, can provide a holistic perspective to investigate the affected biological processes. These approaches enable a comprehensive understanding of the mechanisms of dietary components by examining their effects on a system-wide level[20]. In the present study, we employed multi-omics approaches to investigate the anti-obesity effects of DOP in a DIO mouse model. Our findings suggest that the anti-obesity effects of DOP may be associated with its regulation of LDs in WAT. Covariance network analysis, integrating microbiomics, metabolomics, and transcriptomics, revealed the potential mechanisms through which DOP modulates LDs by regulating the gut microbiota and its metabolites, thereby alleviating obesity.

2. Method and materials

2.1. Preparation of DOP

The extraction method for *Dendrobium officinale* polysaccharides (DOP) was adapted to our previous work[21]. Briefly, the dried stems of Dendrobium officinale were pulverized and immersed sequentially in hexane and 95% ethanol to eliminate non-polar and polar impurities. Crude polysaccharides were then isolated via hydrothermal extraction coupled with ethanol-induced precipitation. To further purify the extract, starch contaminants were enzymatically degraded using α-amylase under controlled thermal conditions, followed by dialysis to remove residual oligosaccharides, salts, and proteolytic fragments. The final refined polysaccharide fraction was obtained through lyophilization.

The final DOP sample contained (94.20 ± 5.79)% neutral sugars, (0.80 ± 0.17)% protein, and (10.81 ± 2.31)% moisture[21]. The average molecular weight of DOP was approximately 312 kDa, with a mannose to glucose ratio of 5.78:1. The backbone of DOP consists of β-Manp units linked by (1→4) glycosidic bonds, with β-Glcp residues also attached via (1→4) linkages[22].

2.2. Animal and diet

Thirty-six five-week-old male C57BL/6J mice (GemPharmatech Co., Ltd, China) were housed under specific pathogen-free conditions with 12-h light-dark cycle, 21-24°C temperature, and 40-70% humidity. Mice were acclimatized for one week after arrival before any treatment, then randomly divided into one normal chow (Beijing Keao Xeli Feed Co., Ltd., China, Cat# 1016706714625204224) fed group (NC, n=12) and two high-fat-diet (Research Diets, Inc., USA, Cat# D12492) fed groups (HFD, n=12 and DOP, n=12). During the experiment, mice were orally gavaged DOP solution (30 mg/mL) at a dose of 300mg/kg/d. During the intervention period, mice in the DOP group were orally gavaged with DOP solution (30 mg/mL in saline) at a dose of 300 mg/kg/day for 9 weeks. Mice in the NC and HFD groups received an equivalent volume of saline by oral gavage. Body weight, average food and water intake were recorded every week during the experiment. All animal experiments were performed under the Guidelines for Care and Use of Laboratory Animals of the National Institutes of Health and were approved by the Institutional Animal Care and Use Committee of Nanchang University (Animal Ethics Approval No. NCULAE-20221030024).

2.3. Metabolic assay

Oral Glucose Tolerance Test (GTT) and Insulin Tolerance Test (ITT) were performed prior to euthanasia, following previously published protocols with slight modifications[23]. For the GTT, glucose (1.5 g/kg body weight for mice) was administered orally after 6 h fasting, and blood samples were obtained from the tail tip at 0, 15, 30, 60, and, 90 min post-administration. For the ITT, insulin (0.8 U/kg body weight for mice) was administered via an intraperitoneal injection after 6 h fasting, and blood samples were obtained from the tail tip at 0, 15, 30, 60, and 90 min post-administration. The glucose levels of tail vein blood samples were measured using a glucose analyzer (ACCU-CHEK Performa, Roche, Mannheim, Germany).

2.4. Sample collection

One day before sacrifice, mouse feces were collected in Eppendorf tubes. Mice were fasted for 12 h before euthanasia by cervical dislocation. Blood was drawn via retro-orbital sinus puncture, allowed to clot for 2 h, and centrifuged at 3000 rpm for 15 min. Serum was then aliquoted into Eppendorf tubes. Epididymal adipose tissues (EAT) were weighed, divided into two portions, and stored in empty Eppendorf tubes or 4% paraformaldehyde-filled Eppendorf tubes, respectively. Colon tissues and colon contents were separated and collected respectively. All samples except fixed tissues were stored at -80°C. Procedures were performed on ice to preserve tissue integrity.

2.5. Determination of serum biomarkers

Serum levels of glucose were determined using glucose kit (glucose oxidase method) (Nanjing Jiancheng Bioengineering Institute, China, Cat# A154-1-1), and serum levels of insulin were determined using Ultra-sensitive mouse insulin ELISA Kit (Crystal Chem, USA, Cat# 90080). All the experiments were performed following the kit manufacturer's instructions.

2.6. Histopathological and immunofluorescence analysis

Collected EAT samples were fixed in 4% paraformaldehyde and embedded in paraffin. For histopathological analysis, Sections (4 μm thick) were cut, deparaffinized, and rehydrated through graded ethanol. Hematoxylin and eosin (H&E) staining was performed to visualize cell morphology. Whole cross sections were scanned using a digital pathology system (Leica Aperio LV1)[21]. For immunofluorescence (IF) analysis[24], sections were mounted on slides and subjected to deparaffinization, rehydration, and antigen retrieval. After blocking nonspecific binding, sections were incubated with primary antibodies against PLIN2 and PLIN3 overnight at 4 °C. Fluorescently labeled secondary antibodies were applied for detection, followed by nuclear counterstaining with DAPI. Sections were then imaged using a digital pathology system. All processes were performed by Wuhan servicebio technology CO., Ltd., China, according to experimental SOP of Servicebio. The calculation of sizes of adipocytes and quantitative analysis of PLIN2 and PLIN3 expressions in EAT was performed using ImageJ.

2.7. RNA sequencing

RNA-seq was performed on EAT samples collected from all available mice[21]. After thawing, each EAT sample was homogenized using a tissue homogenizer and centrifuged to collect the supernatant. Total RNA was extracted using TRIzol reagent, and RNA integrity was assessed with an Agilent 2100 Bioanalyzer. RNA-seq libraries were prepared following PCR amplification. Briefly, mRNA was purified from total RNA, fragmented, and reverse-transcribed to synthesize cDNA. The resulting cDNA underwent end repair, A-tailing, and adaptor ligation, followed by size selection and PCR amplification to generate the final libraries. After quality control, the libraries were sequenced on an Illumina NovaSeq platform to obtain 150 bp paired-end reads. Raw sequencing data were processed to remove adapters, poly-N sequences, and low-quality reads, resulting in high-quality clean data for downstream analyses. Clean reads were mapped to the reference genome using HISAT2, and gene expression levels were quantified as fragments per kilobase of

exon per million mapped fragments (FPKM) using featureCounts. Differential expression analysis was performed with DESeq2, considering genes with a false discovery rate (FDR) < 15% as significant. Functional enrichment of differentially expressed genes was analyzed for Gene Ontology (GO) terms and Kyoto Encyclopedia of Genes and Genomes (KEGG) pathways using the clusterProfiler R package. Additionally, advanced analyses including Gene Set Enrichment Analysis (GSEA) were performed to further explore pathway-level changes.

2.8. Metagenomic sequencing

Metagenomic sequencing was performed on fecal samples collected from all available mice. Fresh fecal pellets were collected from each mouse into sterile EP tubes prior to sacrifice at the experimental endpoint. Samples were immediately snap-frozen in liquid nitrogen and subsequently stored at -80°C until DNA extraction. Bacterial DNA extraction and library preparation were performed according to the manufacturer's protocols. Briefly, 1 μg of DNA per sample was fragmented to approximately 350 bp using a Covaris ultrasonicator. Libraries were constructed from the sheared genomic DNA through end-repair, A-tailing, adapter ligation, and PCR amplification. Qualified libraries were sequenced on an Illumina platform.

Raw sequencing data were preprocessed using Readfq to generate clean reads by removing those containing ≥40 bp of low-quality bases (Q ≤38), ≥10 bp of N bases, or ≥15 bp of adapter overlap. Potential host contamination was filtered by aligning clean reads to a host genome database using Bowtie2 (parameters: --end-to-end --sensitive -I 200 -X 400). Metagenomic assembly was performed using MEGAHIT (--presets meta-large) to obtain scaffolds, which were subsequently broken at N junctions to produce non-N scaftigs. Open reading frames (ORFs) were predicted from scaftigs (≥500 bp) using MetaGeneMark, and ORFs shorter than 100 nt were discarded. A non-redundant gene catalog (unigenes) was constructed from the predicted genes using CD-HIT. Gene abundance in each sample was calculated based on the number of reads mapped to the catalog using Bowtie2, and genes with ≤2 mapped reads in a sample were excluded from further analysis.

For taxonomic annotation, unigenes were aligned against the NCBI NR database using DIAMOND (blastp, e-value ≤1e-5), and taxonomic classifications were assigned using the lowest common ancestor (LCA) algorithm implemented in MEGAN. Functional annotation was performed by aligning unigenes against the KEGG, eggNOG, and CAZy databases, with best blast hit (BBH) results selected. Antibiotic resistance genes were identified by aligning unigenes against the CARD database using the Resistance Gene Identifier (RGI) software (blastp, e-value <1e-30). Subsequent statistical and comparative analyses, including PCA, NMDS, ANOSIM, Metastats, and LEfSe, were performed based on gene, taxonomic, and functional abundance profiles. A Random Forest model was further applied to identify key discriminatory species.

2.9. Untargeted metabolomics

Untargeted metabolomics analysis was performed on serum samples collected from all mice. The specific methodology followed our previously published work[25]. Briefly, serum proteins were precipitated by mixing 100 μL sample with 400 μL acetonitrile (1:4, v/v), followed by vortexing and centrifugation (17,347 × g, 20 min). Chromatographic separation was performed on a Waters HSS T3 C18 column (2.1 × 100

mm, 2 μm) at 40°C with a flow rate of 0.3 mL/min and 5 μL injection volume, using mobile phases of 0.1% formic acid/acetonitrile (positive ion mode) or 10 mM ammonium acetate/acetonitrile (negative ion mode). Metabolites were analyzed via an AB SCIEX TripleTOF 5600+ system operating in both ionization modes (mass range: 50-1000 *m/z*; ion spray voltage: +5500 V for positive/-4500 V for negative), calibrated with manufacturer standards. Data processing comprised metabolite identification using MENTLIN, metabolic pathway enrichment analysis, and dimensionality reduction performed with MetaboAnalyst 6.0.

2.10. Meta-analysis

Meta-analyses of *Plin2* and *Plin3* expression in mice and their homologues in human were conducted through systematic searches of GEO datasets comparing obese cohorts (with/without T2D comorbidity or HFD-fed models) versus lean controls (non-obese/chow-fed groups). Finally, seven human datasets (GSE244118, GSE235696, GSE228892, GSE205668, GSE156906, GSE141432, GSE152991) and seven murine datasets (GSE167311, GSE111412, GSE87854, GSE56038, GSE30247, GSE39549, GSE32095) were selected after screening. GEO2R were used to obtain data including logFC, p-value, and lfcSE for intergroup comparisons. Statistical parameters (logOR, 95% CI, and p-values) were calculated via fixed-effect models.

2.11. Construction of multi-omics network

DOP significantly regulated genes in EAT (FDR<15%), gut microbes (FDR<15%), serum metabolites ($P < 0.05$), and metabolic phenotypes ($P < 0.05$) were used as nodes to construct a multi-omics network. Spearman rank correlations were calculated between all pairs of nodes in each group (HFD and DOP) of the experiment. A combined Fisher's p-value was calculated for each pair based on the correlation p-values from each group, followed by an FDR calculation on the combined p-values. Edges satisfied the following criteria were retained: (i) the sign of correlation coefficients were consistent in the two groups; (ii), the final correlation FDR<5%; (iii) The edges adhered to principles of causality, meaning that for any pair of nodes, the fold changes in the HFD vs. DOP comparison aligned with the sign of their correlation[26, 27]. The network was visualized using Cytoscape.

2.12. Statistical analysis

Values were expressed as mean ± standard error of the mean. Parametric two tail t-test was used to detect statistical difference between any two given groups using GraphPad Prism 10. A p-value lower than 0.05 was considered the threshold for statistical significance.

3. Results

3.1. DOP alleviates HFD-induced adiposity

First, obesity was induced in mice by feeding them an HFD for 9 weeks, with half of the mice simultaneously receiving daily administration of DOP (**Fig. 1A**). As expected, DOP significantly reduced body weight gain (**Fig 1B**) and the weight of EAT (**Fig. 1C**). The proportion of EAT to body weight in the DOP group showed a downward trend compared to the HFD group, but it did not reach statistical significance

(**Fig. 1D**). Additionally, H&E staining of EAT was performed to detect the effects of DOP on adipose tissue hypertrophy (**Fig. 1E**). The distribution of adipocyte size in the DOP group shifted towards smaller sizes compared to the HFD group (**Fig. 1F**). Average adipocyte size was also significantly smaller after DOP treatment (**Fig. 1G**).

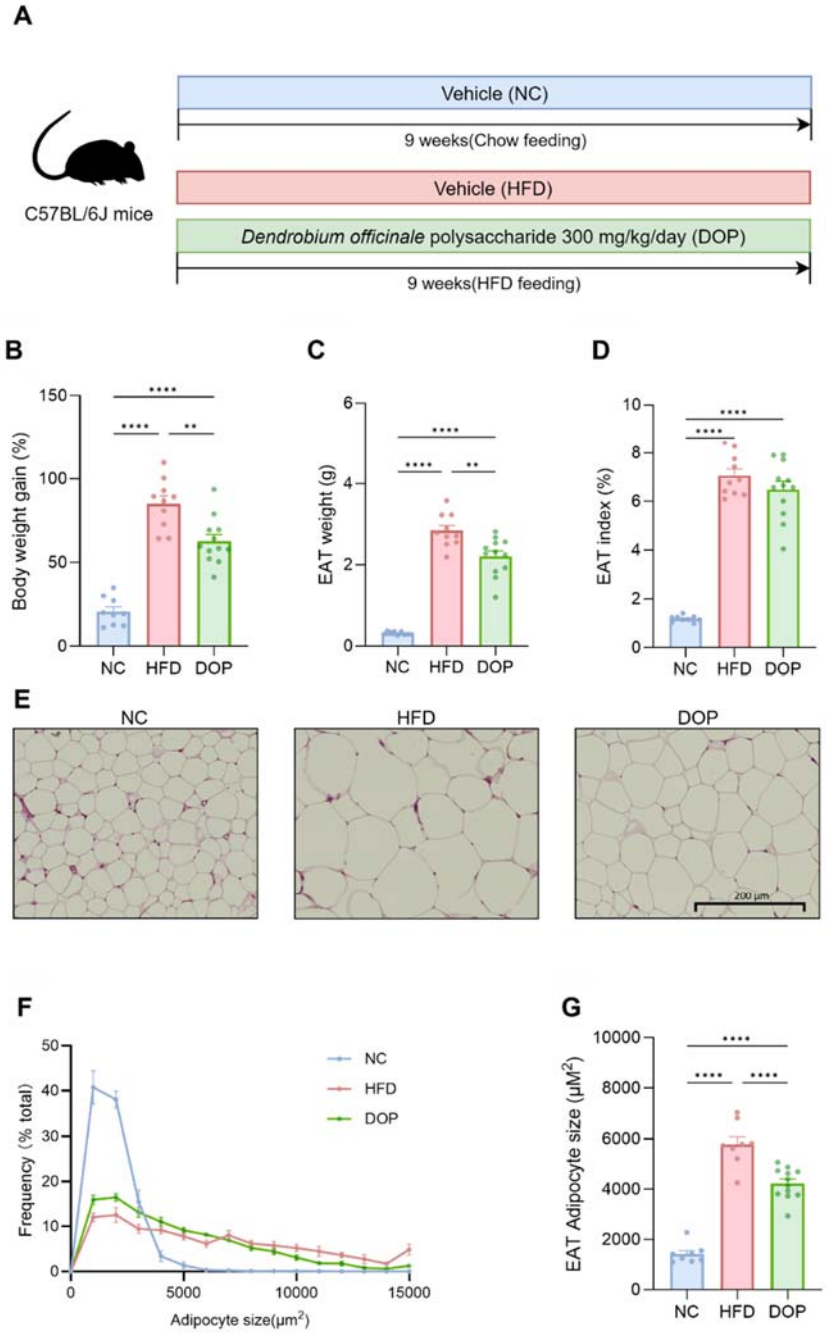

Fig. 1. DOP ameliorates high-fat diet-induced obesity in C57BL/6J mice. (A) Experimental design. **(B)** Body weight gain percentage. **(C)** Epididymal adipose tissue weight (EAT). **(D)** ratio of EAT to body weight. **(E)** H&E staining of EAT. **(F)** Adipocyte size distribution in EAT. **(G)** Mean adipocyte size in EAT. n = 9-12, ***P < 0.001, ****P < 0.0001.

3.2. DOP regulates lipid droplets in the adipocytes of the DIO mice.

RNA-seq showed that DOP significantly regulated 1663 genes in EAT, with 880 upregulated and 783 downregulated (FDR<15%, **Fig. 2A**, **Table S1**). DOP tended to reverse the gene expression changes induced by the HFD, with a binomial test significance of $p = 2.45 \times 10^{-242}$ (**Fig. 2B**). Gene enrichment analysis

restricted to Gene Ontology revealed significant downregulation of pathways associated with LD formation and lipid storage by DOP (**Fig. 2C**). A list of key genes involved in LD formation pathway was upregulated in the HFD group compared to the NC group, but downregulated in the DOP group compared to the HFD group (**Fig. 2D**). Based on the expression levels of these LD-related genes, we calculated an LD score to reflect LD formation from a gene expression perspective. Mice in the HFD group exhibited enhanced LD gene expression compared to normal mice, while DOP treatment significantly reduced this metric (**Fig. 2E**). Of note, the expression levels of *Plin2* and *Plin3*, two important perilipins genes, were significantly upregulated in the HFD mice compared to the NC mice, but were downregulated by DOP treatment (**Fig. 2F-G)**.

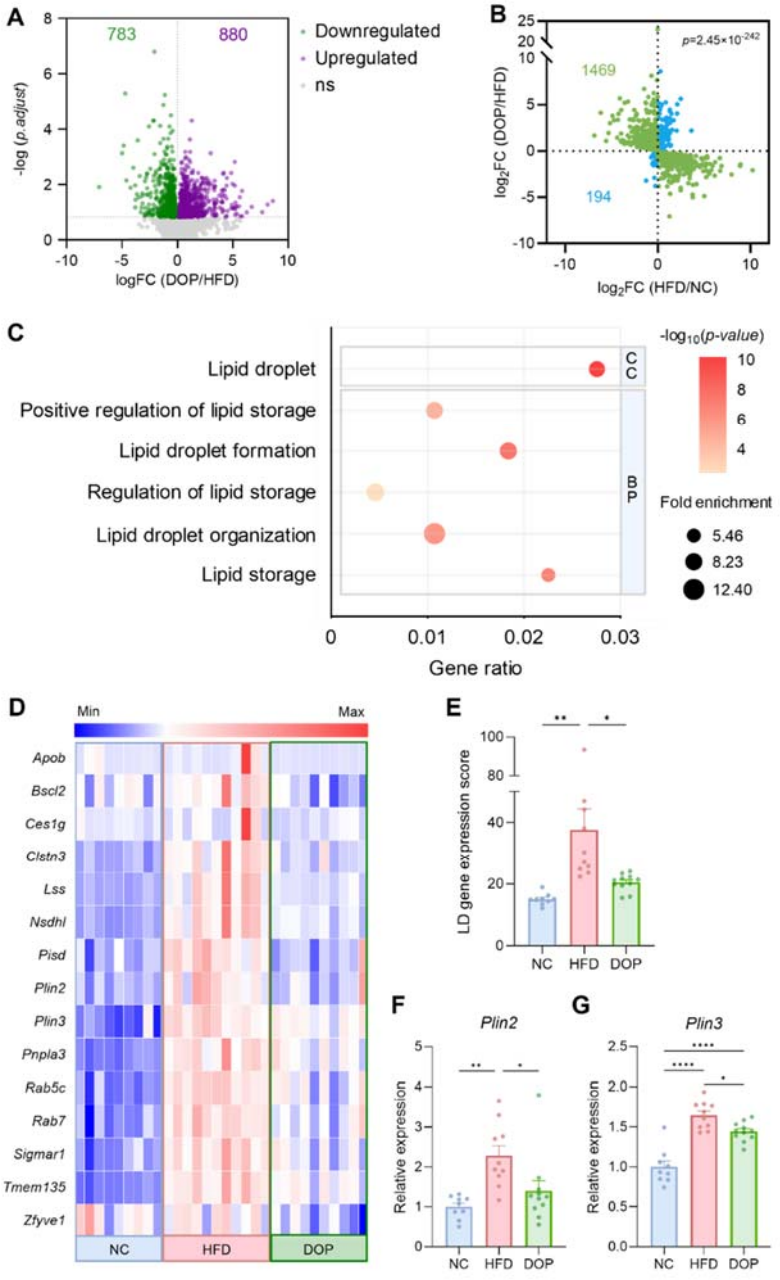

Fig. 2. DOP inhibits lipid droplet-associated gene expression in epididymal adipose tissue of diet-induced obese mice. **(A)** Volcano plot of genes regulated by DOP treatment (FDR<15%). **(B)** Relationship between the regulation of DOP and HFD on gene expression. **(C)** Gene enrichment analysis restricted to Gene Ontology on DOP downregulated genes. **(D)** Heatmap showing the expression of genes in lipid droplet pathway. **(E)** The genes in panel D were first normalized by their mean expression values, and then summed to reflect the overall expression level of LD-related genes. **(F-G)** Relative expression of *Plin2* (F) and *Plin3* (G) in EAT. n = 9-12, *P < 0.05, **P < 0.01, ****P < 0.0001.

Immunofluorescence staining was performed to visualize the expression of perilipin 2 (PLIN2, red) and perilipin 3 (PLIN3, green) at protein level in the WAT sections from NC, HFD, and DOP groups (**Fig. 3A**). Compared to the NC group, the HFD group exhibited significantly increased fluorescence signals for PLIN2 and PLIN3. Moreover, the co-localization of PLIN2 and PLIN3 was markedly enhanced in the HFD group, as indicated by an increase in yellow regions. In contrast, DOP treatment effectively reduced the co-localization signals of PLIN2 and PLIN3. Quantitative analysis further confirmed that DOP intervention significantly decreased the protein levels of PLIN2 and PLIN3 compared to the HFD group (**Fig. 3B-C**).

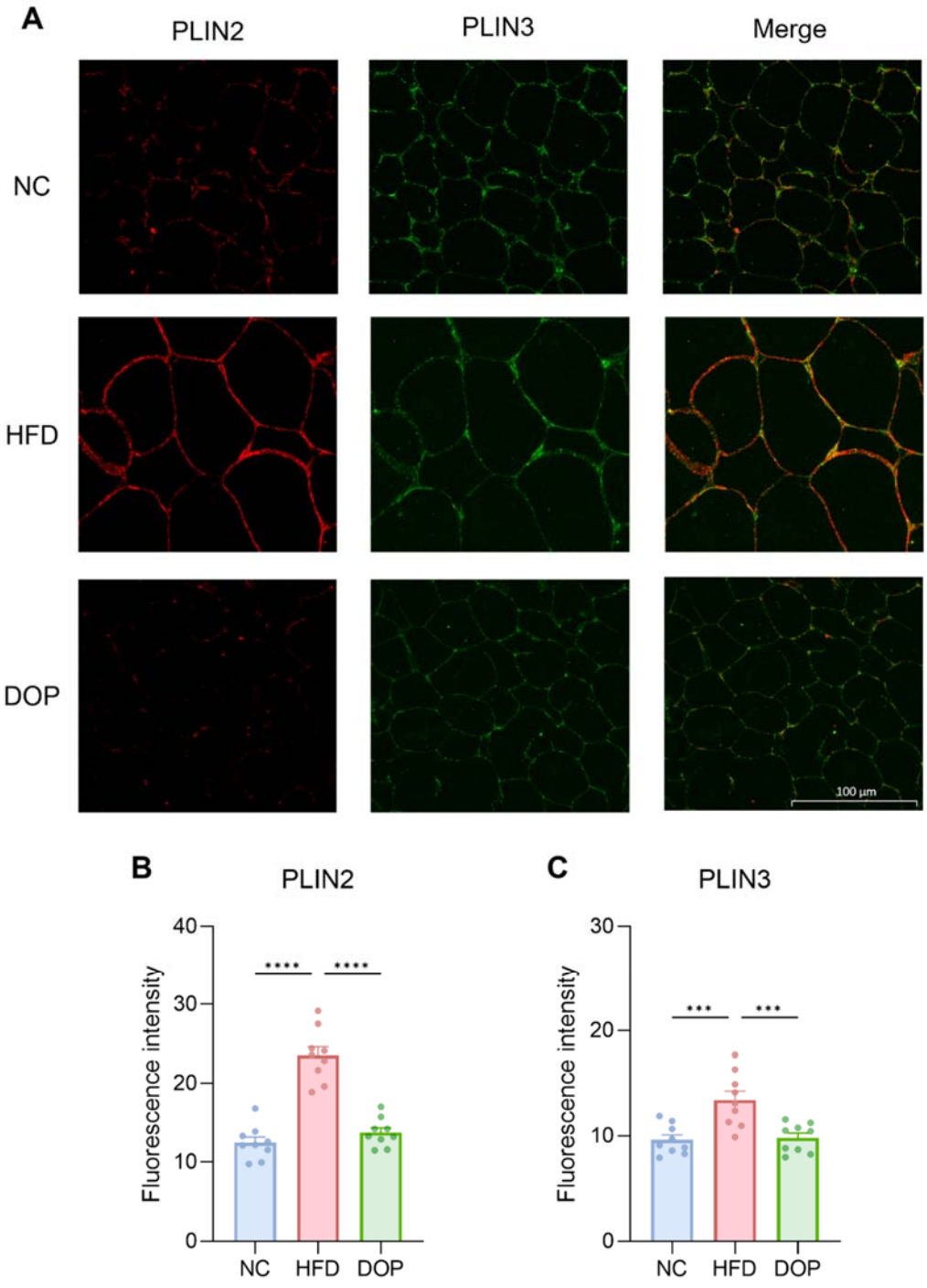

Fig. 3. Immunofluorescence analysis showing the influence of DOP treatment on the protein levels of PLIN2 and PLIN3**. (A)** Representative immunofluorescence images of PLIN2 (red) and PLIN3 (green) in EAT. **(B-C)** Quantification of PLIN2 (B) and PLIN3 (C) fluorescence intensity in EAT. $n = 9$, ***$P < 0.001$, ****$P < 0.0001$.

3.3. Perilipins are upregulated in both obese mice and humans

As our animal experiments demonstrated that key perilipins, PLIN2 and PLIN3, were significantly upregulated in the adipose tissue of obese mice, we further investigated whether this phenomenon is a common feature of obesity through meta-analyses. To this end, we downloaded gene expression data of adipose tissue from both DIO mice and obese humans available in the GEO database and conducted meta-analyses (**Table S2**).

In DIO mice, as shown in **Fig. 4A-B**, *Plin2* expression showed a slight upward trend (OR=1.5, 95% CI: 0.74-3.09) but did not reach statistical significance (p=0.26), as indicated by the fixed-effect model. In contrast, *Plin3* was significantly upregulated (OR=71.75, 95% CI:12.12-424.15, $p=2.43\times10^{-6}$), suggesting robust evidence of its association with obesity in mice.

Similarly, in the adipose tissue of obese humans (**Fig. 4C-D**), PLIN2 showed an upward trend (OR=1.33, 95% CI: 0.92-1.92) with borderline statistical significance (p=0.13), while PLIN3 was significantly upregulated (OR=6.20, 95% CI: 4.05-9.50, $p=5.08\times10^{-17}$), supporting the association of PLIN3 with obesity in humans.

Overall, these findings highlight a strong and consistent upregulation of PLIN3 in obesity across species, while the upregulation of PLIN2 appears to be more variable and context-dependent.

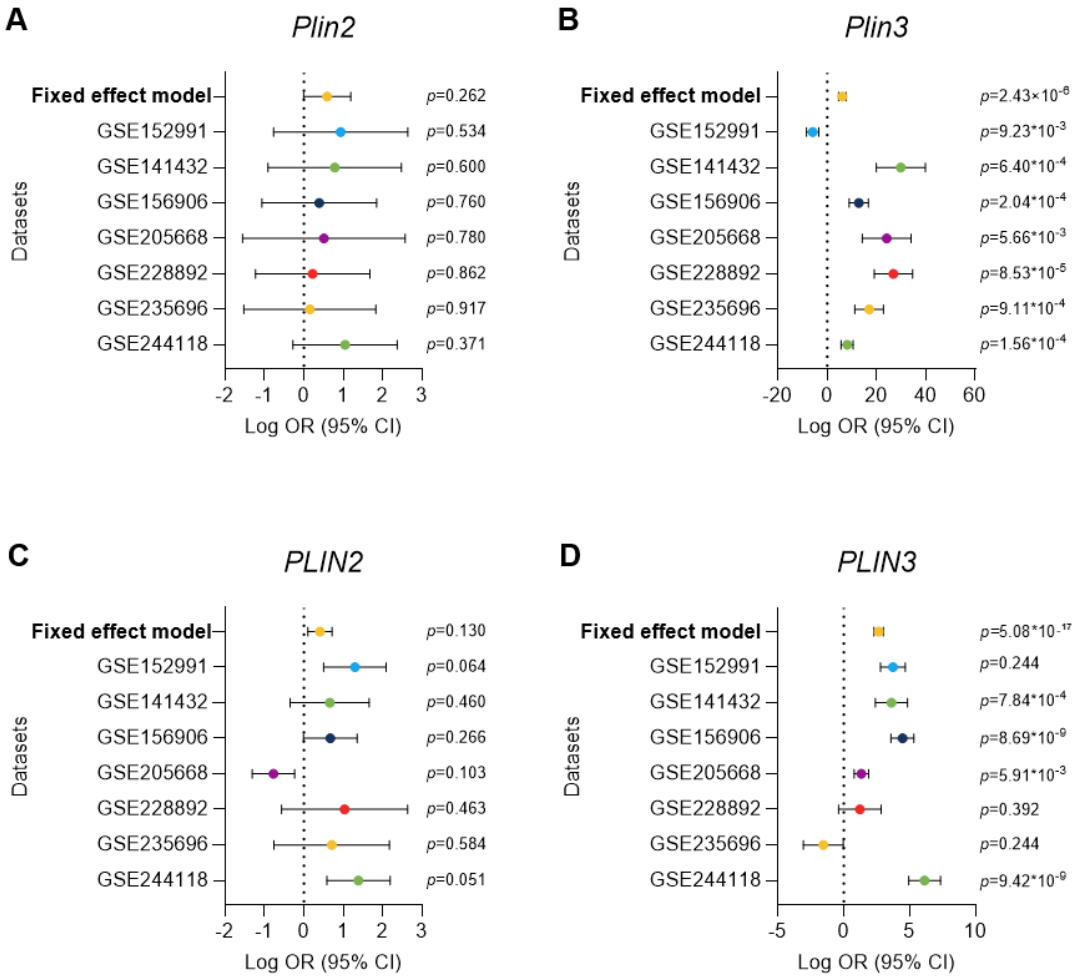

Fig. 4. Meta-analysis of lipid droplet-associated genes in EAT and obesity. (A-B) Forest plots of *Pin2* (A) and *Plin3* (B) expression in mouse datasets. **(C-D)** Forest plots of *PLIN2* (c) and *PLIN3* (D) expression in human datasets.

3.4. Lipid droplet positively correlates with metabolic parameters

To investigate whether the downregulation of LDs by DOP contributes to its ability to improve obesity-related metabolic disorders, we analyzed the association between LD-associated genes and various metabolic parameters including adipocyte size, body weight gain, EAT weight, glucose tolerance, and insulin tolerance. A notable observation is that these genes generally exhibited a positive correlation with these metabolic parameters (**Fig. 5A**). Furthermore, the LD gene expression score also showed significant positive correlations with body weight, EAT weight, blood glucose, GTT-AUC, insulin, and ITT-AUC (**Fig. 5B-G**). These results suggest that LD expansion may lead to adipose tissue hypertrophy and impair glucose metabolism homeostasis.

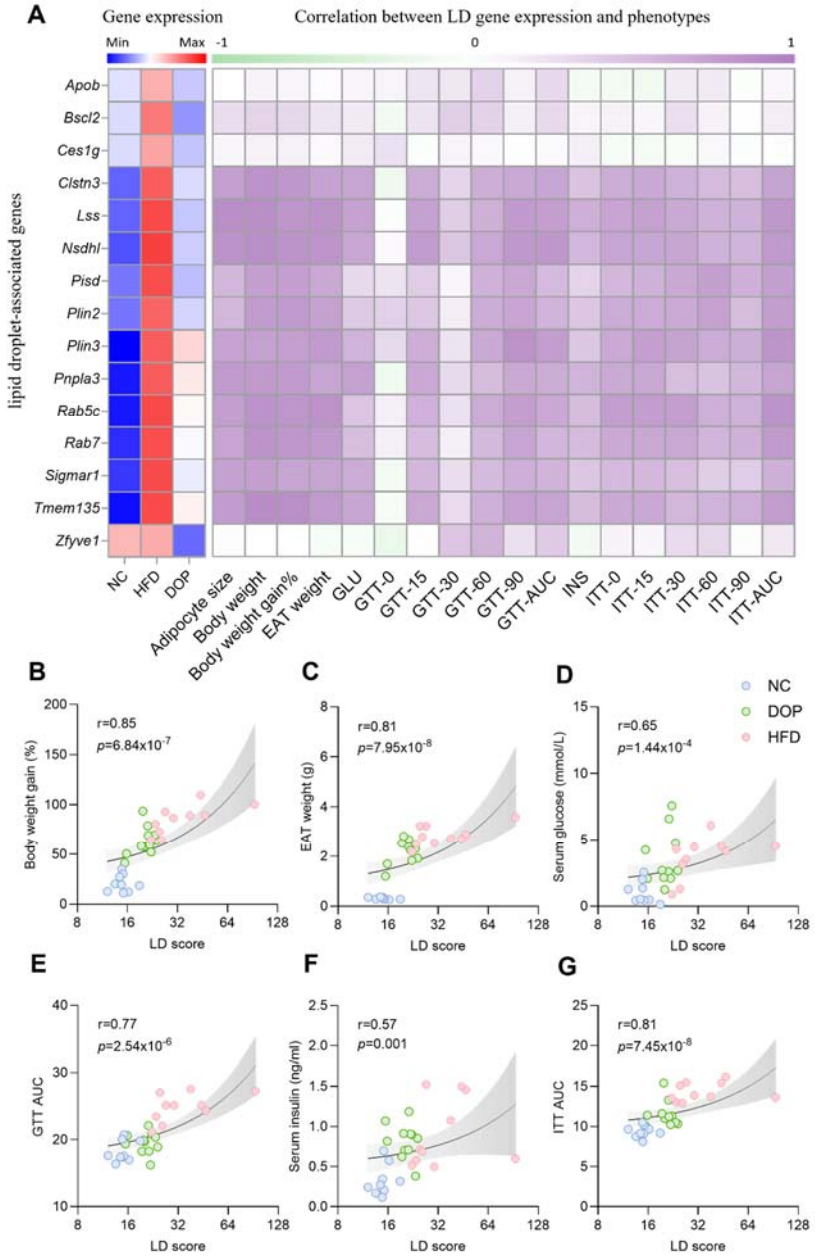

Fig. 5. The expressions of lipid droplet-related genes in EAT correlate with various metabolic parameters. (A) A heatmap showing the expression patterns of genes in the lipid droplet pathway and their correlation with various metabolic parameters. The left panel shows the expression levels of LD-related genes across the three groups. The right panel shows the correlations between the expression levels of these genes and phenotypic parameters. **(B-G)** Scatter plots showing the correlation between lipid droplet gene expression and various metabolic parameters. n = 9-12.

3.5. DOP downregulates the lipid biosynthesis and storage process in adipose tissue

LDs are the primary sites for lipid storage in adipocytes. Since DOP significantly inhibited LD formation, we subsequently investigated the effects of DOP on lipid synthesis and storage-related processes in EAT. Firstly, Gene Set Enrichment Analysis (GSEA) revealed that the lipid biosynthesis and lipid storage pathways were significantly inhibited by DOP **(Fig. 6A-B)**. Compared to normal diet, HFD markedly increased the expression of genes associated with these pathways, while DOP significantly suppressed their expression relative to the HFD group **(Fig. 6C-D)**. Leptin, which suppresses appetite and lipid synthesis, is compensatorily overexpressed during DIO due to leptin resistance[28]. FABP1 is involved in the intracellular transport and storage of long-chain fatty acids and other lipid molecules[29]. FASN serves as a key enzyme in *de novo* fatty acid synthesis, catalyzing the conversion of acetyl-CoA and malonyl-CoA into long-chain saturated fatty acids[30]. LDL-R is responsible for clearing LDL from the bloodstream and transporting it into cells[31]. These key genes related to lipid synthesis and storage were significantly upregulated in HFD-fed mice, whereas DOP markedly suppressed their expression (**Fig. 6E**). Furthermore, DOP also regulated the expression of genes associated with adipocyte differentiation. For instance, DOP significantly inhibited *Cebpb*, which promotes adipocyte differentiation[32]. The HFD-induced changes in *Dio2* and *Klf5* expression were also significantly reversed by DOP. Additionally, *Pparg* showed an upward trend with DOP treatment, though the change was not statistically significant (**Fig. 6F**). These results suggest that DOP may alleviate LD expansion through regulating lipid biosynthesis and storage process.

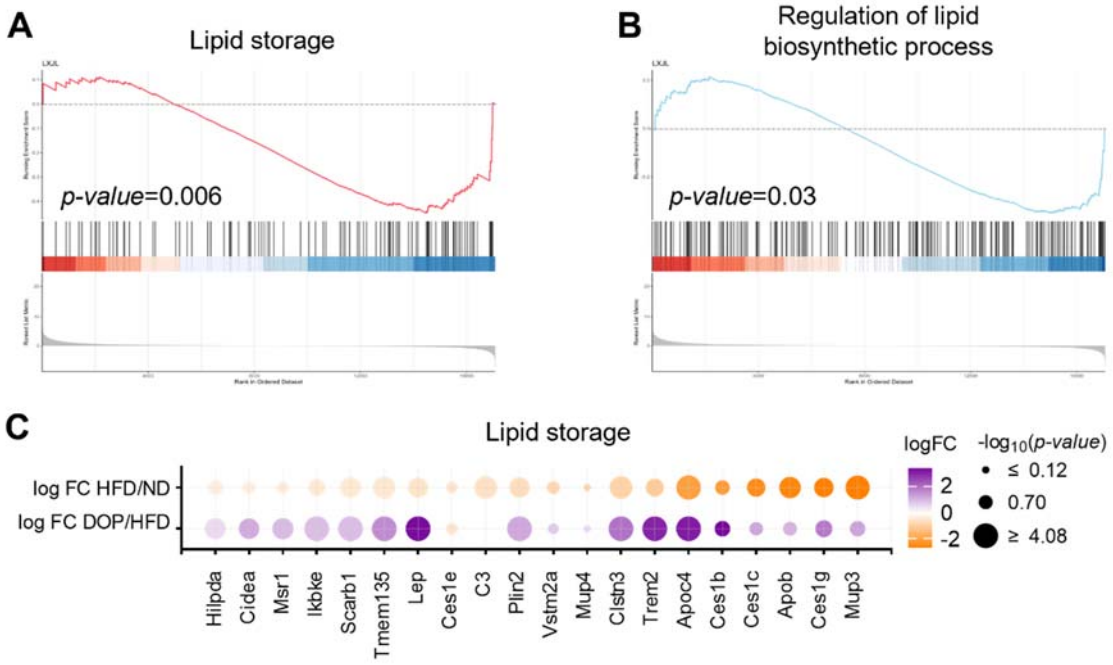

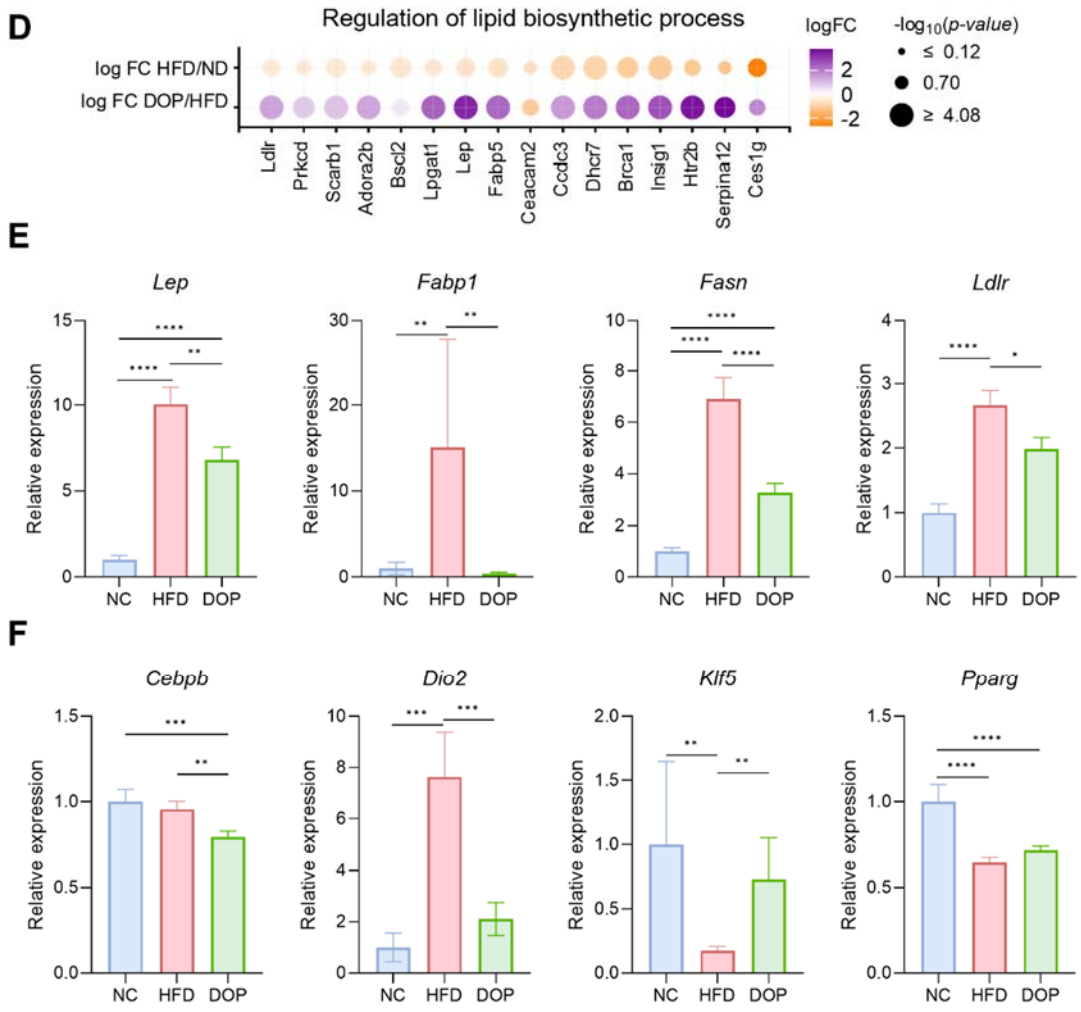

Fig. 6. DOP inhibits lipid biosynthesis and storage in the EAT of HFD-fed mice. (A-B) Results of GSEA show that DOP inhibit the lipid storage pathway (A) and the regulation of lipid biosynthesis pathway (B). **(C-D)** Regulation of DOP on the key genes in the pathways described in panel A and B, respectively. **(E-F)** Relative expression of subsets of the genes associated with lipid storage & biosynthesis (E) and adipocyte differentiation (F). $n = 9 – 12$, $^{*}P < 0.05$, $^{**}P < 0.01$, $^{***}P < 0.001$, $^{****}P < 0.0001$.

3.6. DOP stimulates Wnt signaling pathway in WAT of DIO mice.

The inhibitory effects of DOP on lipid synthesis and storage may result from its upregulation of the Wnt signaling pathway, which suppresses adipocyte differentiation. Indeed, GSEA showed that DOP supplementation significantly activated the Wnt signaling pathway in EAT (**Fig. 7A**). Compared to mice on a NC diet, the expression of Wnt pathway-related genes was generally reduced in HFD-fed mice, whereas DOP intervention significantly increased their expression (**Fig. 7B**). Key members of the Wnt family genes, including *Wnt5b*, *Wnt6*, and *Wnt7b*, were significantly downregulated in the EAT of DIO mice, but their expression was markedly upregulated following DOP intervention (**Fig. 7C**). *Axin2*, a negative regulator of Wnt signaling, facilitates the degradation of β-catenin to prevent excessive activation of the pathway[33]. Meanwhile, *Gata2* and *Gata3*, as downstream transcription factors of the Wnt signaling pathway, play critical roles in inhibiting adipocyte differentiation[34]. We observed that HFD feeding reduced the expression of these genes, whereas DOP supplementation upregulated their expression (**Fig. 7D-F**). These findings suggest that DOP may inhibit adipocyte differentiation, possibly through activation of the Wnt signaling pathway.

In addition, we used immunofluorescence to visualize Wnt proteins in EAT. The results showed that in DIO mice, the fluorescence signals of Wnt6 and Wnt7B were significantly decreased (**Fig. 8A**). This is consistent with previous reports that HFD-induced obesity leads to reduced Wnt signaling activity in adipose tissue, which promotes preadipocyte differentiation and accelerates adipose tissue expansion and obesity progression[35]. In contrast, the fluorescence signals of Wnt6 and Wnt7B in the EAT of DOP-treated mice were much stronger than those in the HFD group (**Fig. 8B-C**), indicating that DOP may inhibit adipose tissue expansion and obesity development by upregulating the Wnt signaling pathway.

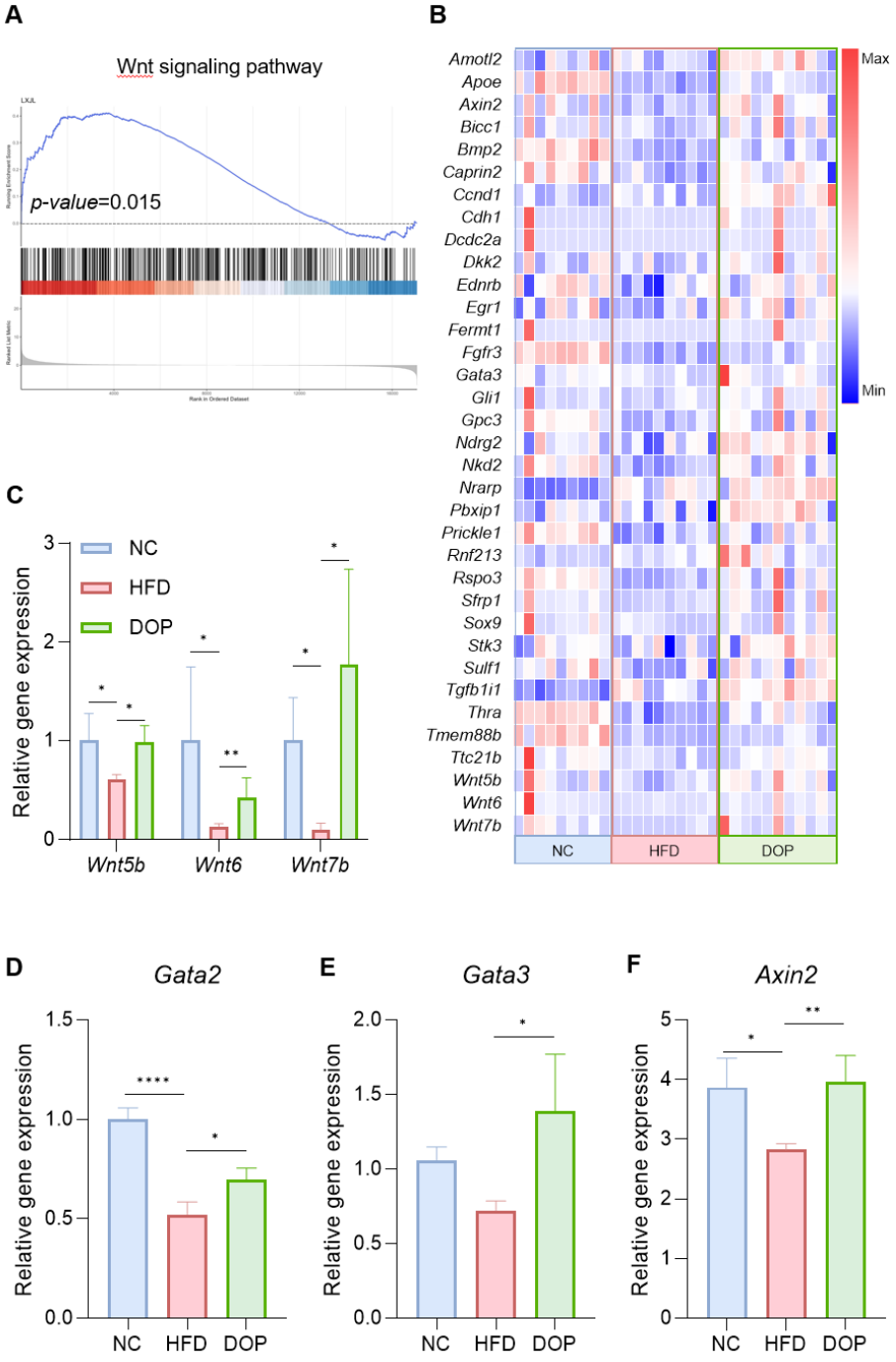

Fig. 7. DOP promotes Wnt signaling in EAT of HFD-fed mice. (A) Results of GSEA showing that DOP significantly enhanced Wnt signaling. **(B)** A heatmaps showing the expression of genes in Wnt signaling pathway. **(C)** Relative expression of *Wnt5b*, *Wnt6*, and *Wnt7*. **(D-F)** Relative expression of *Gata2*, *Gata3*, and *Axin2*. n = 9-12, *$P < 0.05$, **$P < 0.01$, ****$P < 0.0001$.

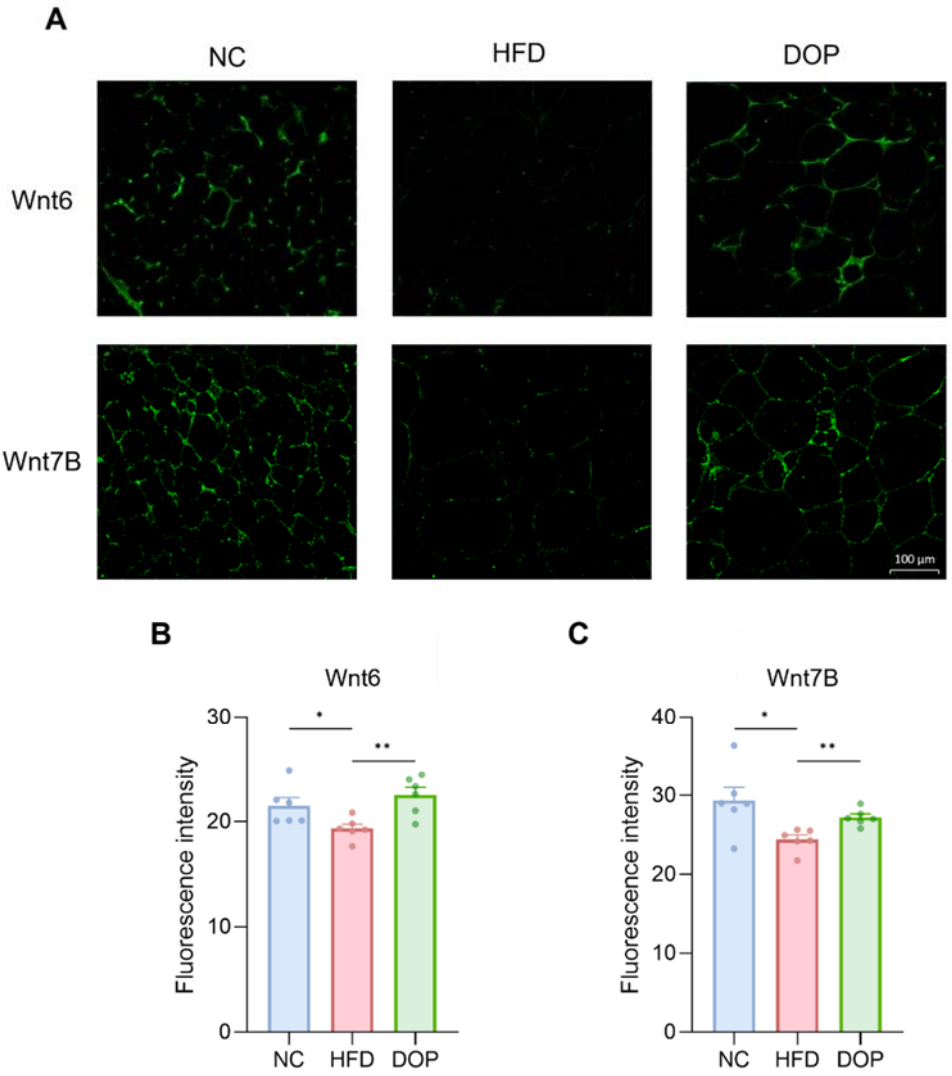

Fig. 8. Immunofluorescence analysis of Wnt6 and Wnt7B protein expression in epididymal adipose tissue. (A) Representative immunofluorescence images showing Wnt6 and Wnt7B expression. (B-C) Quantitative comparison of Wnt6 and Wnt7B protein levels among different groups of mice. n =6, *$P < 0.05$, **$P < 0.01$.

3.6. DOP alleviates HFD-induced gut microbiota dysbiosis

As a dietary fiber, DOP may regulate host metabolism by modulating the gut microbiota. Metagenomic analysis showed that DOP tended to reverse HFD-induced changes in gut microbial abundance. Microbes that were downregulated in the HFD group compared to the NC group tended to be upregulated by DOP, and vice versa (**Fig. 9A**). Notably, 331 microbial species (e.g., *Bifidobacterium castoris*, *Faecalibacterium sp.* AF10-46, *Prevotella dentasini*) were present only in the ND group and absent in the HFD group, but reappeared after DOP intervention (**Table S3**). Conversely, 51 species (e.g., *Blautia sp. OM07-19*, *Clostridium drakei*, *Campylobacter coli*.) that were absent in the ND group but present in the HFD group disappeared following DOP treatment (**Fig. 9B**).

Specifically, we observed some microbes downregulated by HFD but upregulated by DOP showed a negative correlation with LD scores and tended to negatively correlate with metabolic parameters such as body weight gain, GTT-AUC, and ITT-AUC. Conversely, some microbes upregulated by HFD but downregulated by DOP showed a positive correlation with LD scores and were more likely to positively

correlate with metabolic parameters (**Fig. 9C**). This phenomenon suggests that DOP may inhibit LD growth by modulating the gut microbiota, thereby improving the metabolic phenotype.

To identify the microbes potentially mediating the effects of DOP, we analyzed those with high abundance, upregulated by DOP, and significantly negatively correlated with LDs. As shown in **Fig. 9D**, two bacteria from the *Bifidobacterium* genus, *B. pseudolongum* and *B. choerinum*, exhibited significantly reduced abundance after HFD feeding, which was notably restored by DOP supplementation (**Fig. 9E-F**). Furthermore, their abundance was significantly negatively correlated with LD. These two candidate bacteria may play a key role in mediating the effects of DOP.

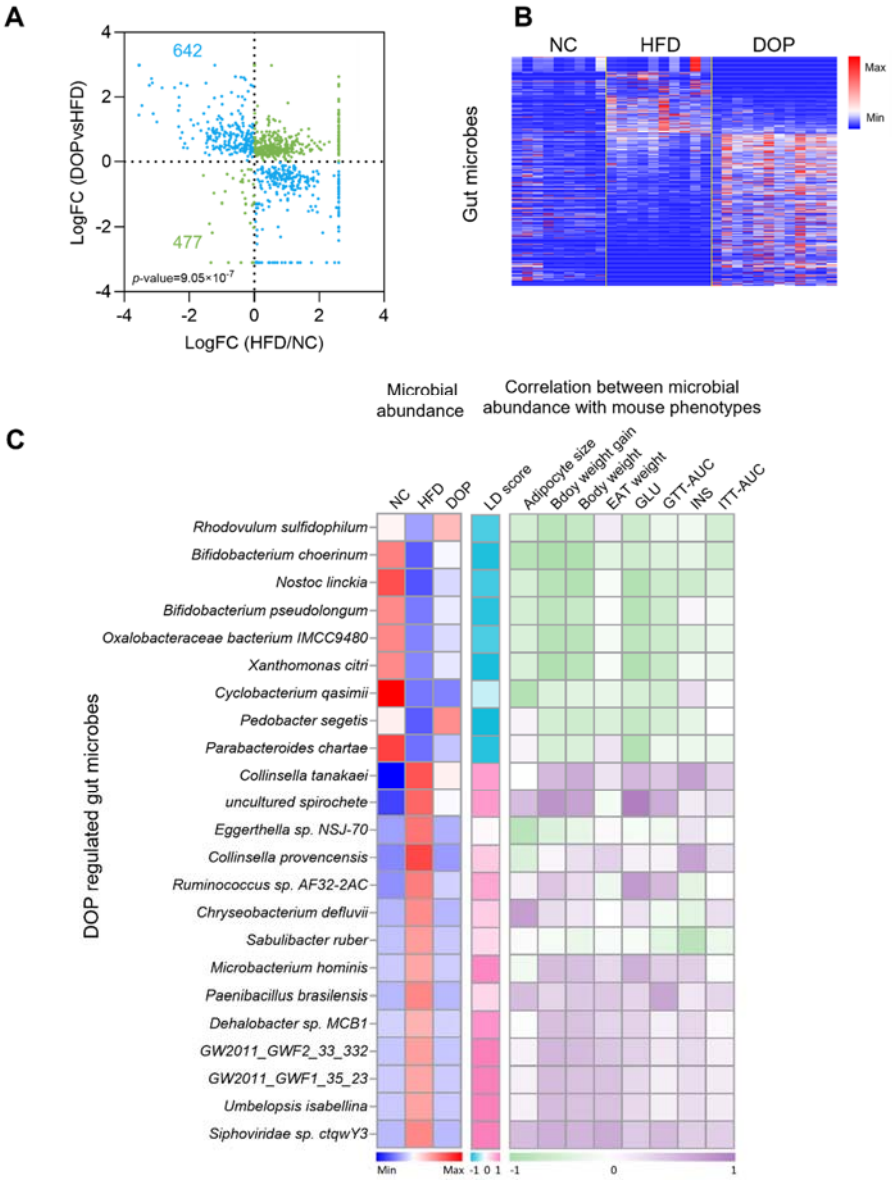

Fig. 9. The regulatory effects of DOP on diet-induced gut microbiota dysbiosis and their relationship with lipid droplet formation and metabolic phenotypes. (A) Scatter plot depicting the relationships between the regulation of DOP and HFD on the gut microbes. (B) Heatmap depicting the abundance of gut microbes that were significantly regulated by DOP (FDR<15%). (C) A heatmap showing the abundance of gut microbes regulated by DOP, with their levels demonstrating a concordant correlation with LD expansion and metabolic parameters. (D) A scatter plot of gut microbes (The x-axis and y-axis represent the p-value of the correlation and the correlation coefficient between microbial abundance and LD gene expression, respectively. The color of the points indicates the fold change of microbes regulated by DOP, while the size of the points represents the average abundance of the microbes in the feces). (E-F) Abundance of *Bifidobacterium pseudolongum* (E) and *Bifidobacterium choerinum* (F). GLU, fasting serum glucose; GTT-AUC, glucose tolerance test area under curve; INS, fasting serum insulin; ITT-AUC, insulin tolerance test area under curve. n = 9-12, ****P < 0.0001.

3.7. DOP shifts the profiles of circulating metabolites in DIO mice

Given that metabolites are one of the primary mechanisms through which the gut microbiota influences host metabolism[36], we performed untargeted metabolomic analysis on mouse sera (**Table S4**). Dimensionality reduction analysis revealed a clear separation among the NC, HFD, and DOP groups in the low-dimensional space (**Fig. 10A-C**). This suggests that DOP supplementation significantly modulates the serum metabolite profiles.

We identified a list of metabolites whose concentration changes in DIO mice were reversed by DOP and showed concordant correlations with the expression of LD-related genes. Metabolites upregulated by DOP tended to be negatively correlated with the phenotypic outcomes including adipocyte size, body weight gain, GTT-AUC, and ITT-AUC, while those downregulated by DOP tended to be positively correlated with these phenotypes (**Fig. 10D**).

Acylcarnitine levels reflect the activity of fatty acid β-oxidation. While some studies suggest that excessive accumulation of plasma acylcarnitines may indicate mitochondrial dysfunction[37], others have reported that long-chain acylcarnitine levels increase in HFD-fed rats following exercise or dietary restriction and show a positive correlation with insulin sensitivity[38]. In this study, acylcarnitines such as 9,12-Hexadecadienoylcarnitine, 3-Hydroxy-5,8-Tetradecadiencarnitine, 3-Hydroxyhexadecadienoylcarnitine, and L-Palmitoylcarnitine were downregulated in HFD-fed mice but upregulated by DOP, and they exhibited negative correlations with metabolic disorder-related phenotypes (**Fig. 10D**). These results suggest that DOP-regulated serum metabolites may potentially mediate the regulatory effects of DOP on LD-related genes and, ultimately, on the metabolic phenotype.

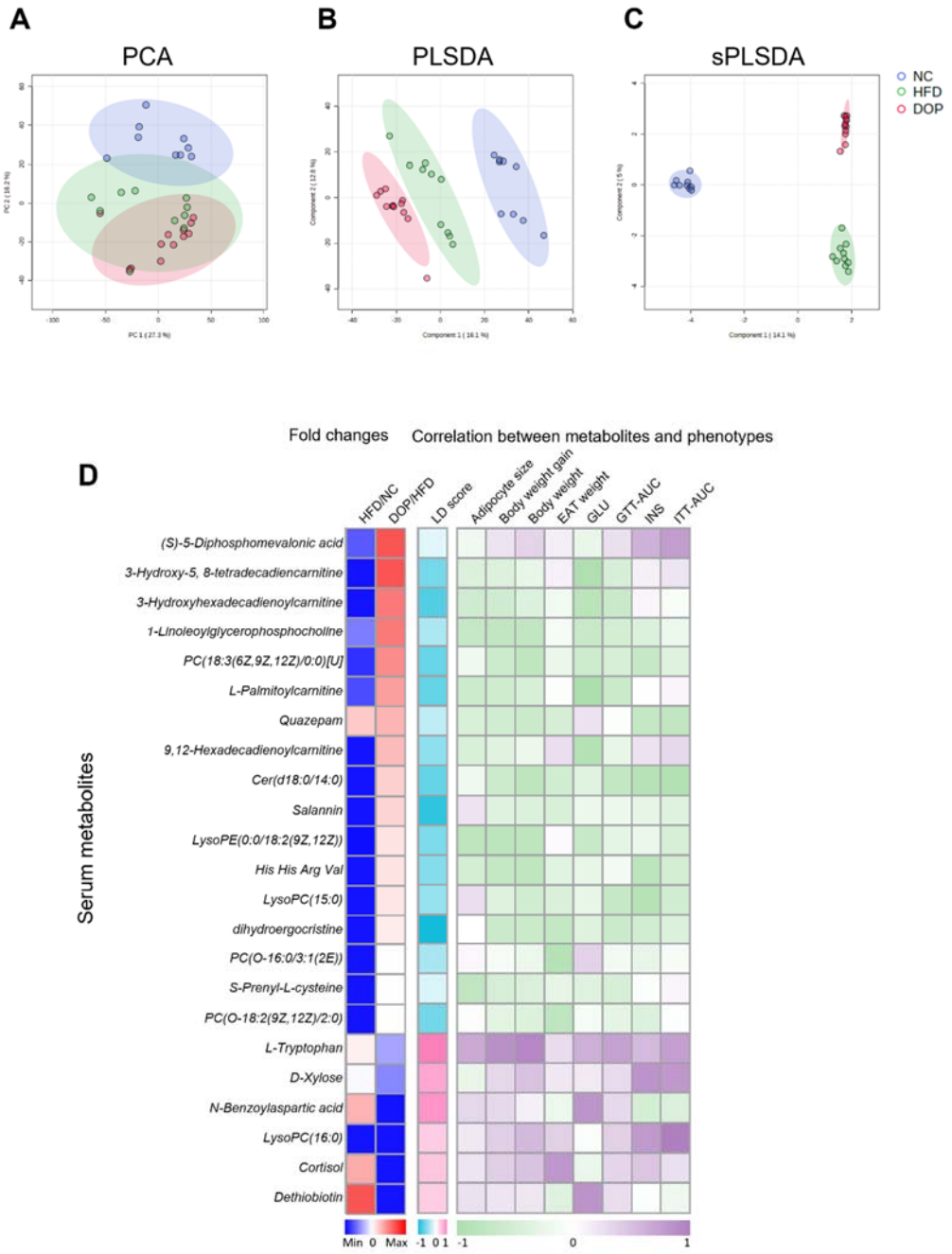

Fig. 10. The metabolites regulated by DOP may potentially mediate its regulatory effects on LD-related genes and metabolic phenotypes. (A-C) PCA (Principal Component Analysis), PLSDA (Partial Least Squares Discriminant Analysis) and sPLSDA (Sparse PLSDA) of serum metabolites. (D) A heatmap depicting DOP-regulated metabolites and their correlations with the expression of LD-related genes and metabolic parameters. GLU, fasting glucose; GTT-AUC, glucose tolerance test area under curve; INS, fasting insulin; ITT-AUC, insulin tolerance test area under curve. n = 9-12.

3.8. DOP regulates metabolism by modulating the gut microbiota and its metabolites

To comprehensively visualize the information flow influenced by DOP, we performed a covariance network analysis to integrate multi-omics data, including the gut microbiome, serum metabolome, adipose tissue transcriptome, and phenotypic data from mice. The constructed network includes 387 gut microbes, 176 serum metabolites, 1303 genes in EAT, and 16 metabolic parameters. As shown in **Fig. 11**, the microbial subnetwork has minimal direct connections with the phenotypic subnetwork. Instead, it primarily influences gene expression in adipose tissue, either directly or via metabolites, ultimately affecting the metabolic parameters of mice. Therefore, based on the previous findings and network analysis results, it can

be inferred that by modulating the gut-adipose tissue axis, DOP can potentially activate the Wnt signaling pathway in WAT, suppress lipid synthesis and storage, inhibit LD expansion, and ultimately mitigate DIO (**Fig. 12**).

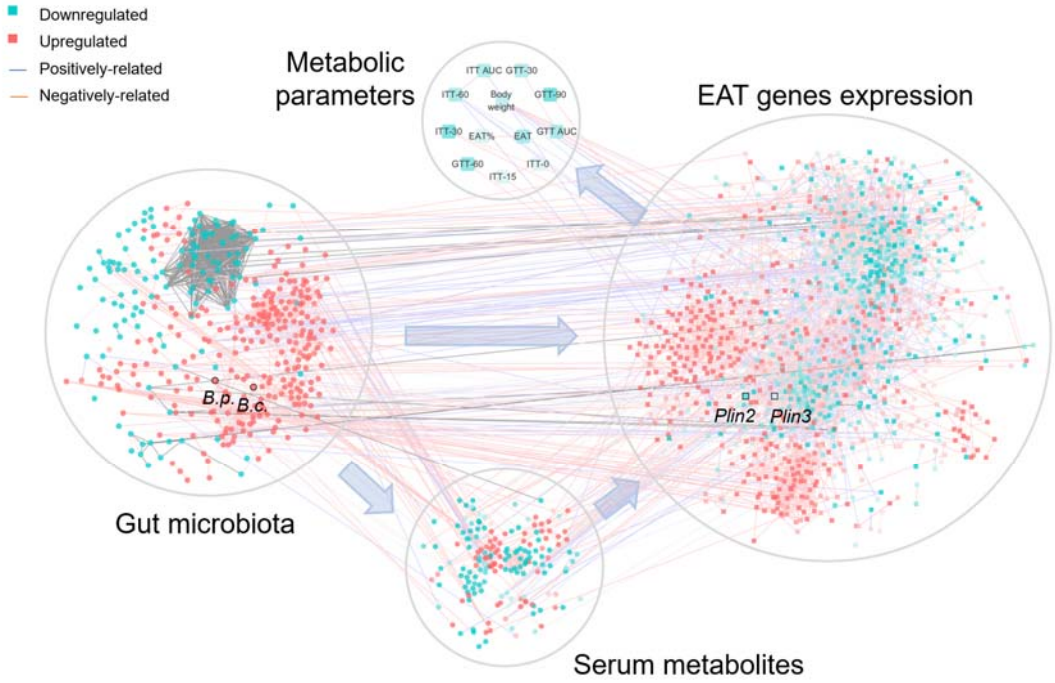

Fig. 11. A multi-omics covariance network modeling the information flow under DOP treatment in HFD-induced obese mice. The nodes in the figure represent gut microbes, serum metabolites, gene expressions, or metabolic phenotypes significantly regulated by DOP. The colors of the nodes correspond to the direction of regulation by DOP. The edges represent the Spearman correlation between two nodes, with the edge colors reflecting the sign of the correlation. The network was constructed according the principle of causality (refer to the Methods section for details).

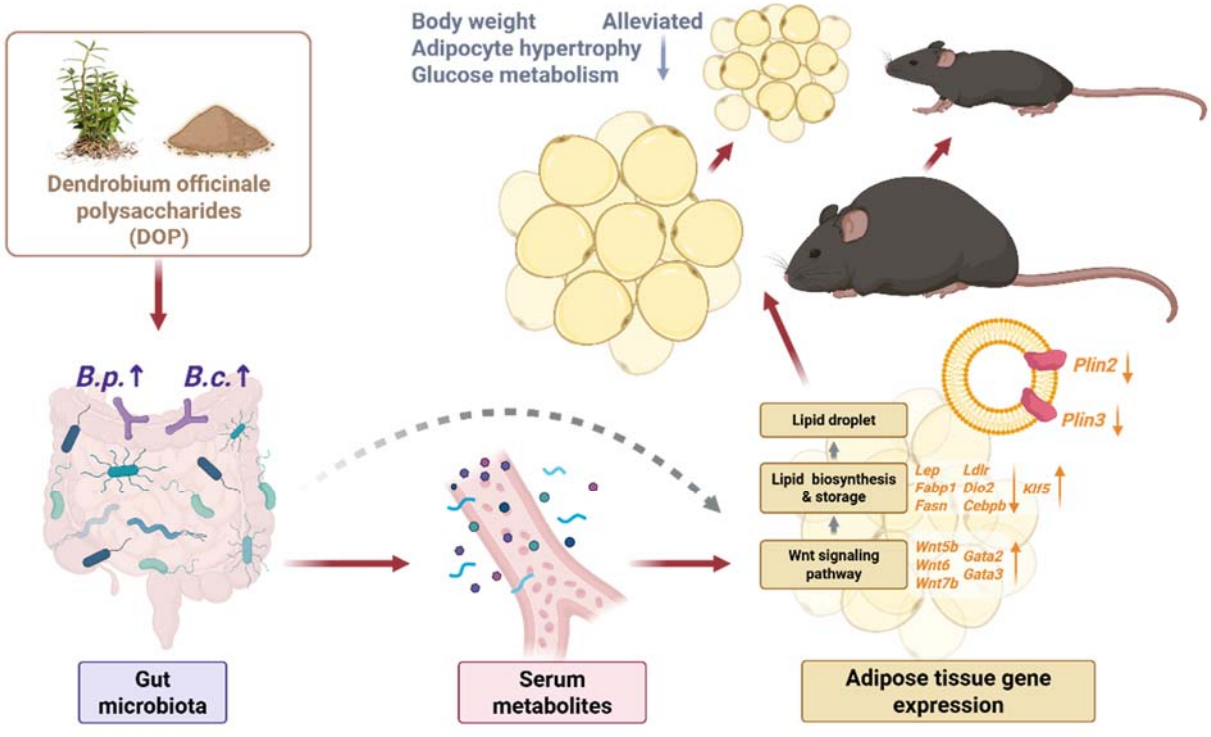

Fig. 12. Through the gut-adipose tissue axis, *Dendrobium officinale* polysaccharides activate Wnt signaling, thereby suppressing lipid synthesis and lipid droplet expansion, ultimately alleviating diet-induced obesity**.**

4. Discussion

The anti-diabetic effect of DOP has been demonstrated in several studies[39]. In the gut, DOP regulates gut microbiota composition, increases short-chain fatty acid (SCFA) levels in feces, strengthens intestinal barrier function, and reduces the secretion of the pro-inflammatory cytokine TNF[40]. In the liver, DOP inhibits gluconeogenesis and glycogenolysis, promotes glycogen synthesis, and reduces the expression of pro-inflammatory cytokines TNF and IL-6 [40, 41]. In the pancreas, DOP lowers the proportion of α-cells while increasing β-cell proportions, thereby enhancing insulin secretion[40, 41]. In adipose tissue, DOP suppresses the expression of pro-inflammatory cytokines TNF and IL-6, while promoting the expression of anti-inflammatory cytokines IL-10 and IL-4[42]. These findings highlight the multifaceted therapeutic potential of DOP in managing T2D.

However, obesity is a major risk factor for T2D, yet the mechanisms through which DOP prevents obesity remain unclear. It is reported that an HFD induces inflammation first in WAT and subsequently in the liver[43]. Furthermore, another study found that an HFD causes insulin resistance first in the liver and then in muscle tissue[44]. These findings suggest that the sequence of significant pathological changes induced by diet may be WAT, followed by the liver, and then muscle. Therefore, this study focuses on the regulatory effects of DOP on WAT to investigate its anti-obesity mechanisms.

Compared to subcutaneous fat, visceral fat has a more significant impact on obesity-related metabolic diseases[45]. During obesity, LDs expand to accommodate the increased storage capacity[46]. In this study, DOP could significantly reduce diet-induced hypertrophy and hyperplasia of visceral fat. Moreover, DOP also inhibited the LD formation and lipid storage processes in EAT.

Perilipins are associated with the formation, stabilization, and lipid metabolism of LDs[17]. PLIN2 reduces adipose triglyceride lipase (ATGL) localization to lipid droplets and slows rates of lipolysis[47]. Under nutrient deprivation, AMP-activated protein kinase (AMPK) catalyzes the phosphorylation of PLIN2, which facilitates access of ATGL and lipophagy-related proteins to LDs, initiating the hydrolysis of stored lipids[48]. PLIN3 is rapidly recruited to LDs upon fatty acid exposure, and its knockdown hinders their formation[49]. Additionally, PLIN3 knockdown prevents diet-induced hepatic steatosis and decreases the secretion of very low-density lipoprotein[50, 51].

We found that an HFD could upregulated the expression of *Plin2* and *Plin3* in mouse WAT at both mRNA and protein levels, with their levels showing significant positive correlations with various metabolic parameters related to obesity and glucose metabolism. This suggests that these perilipins may play a significant role in DIO. To determine the generality of this phenomenon, we conducted a meta-analysis of multiple animal studies and human data. The results revealed that *Plin2* consistently showed an upward trend in various datasets, while Plin3 exhibited a significant association with obesity in both mouse and human adipose tissues. Additionally, DOP intervention effectively reduced the expression of *Plin2* and *Plin3*, thereby inhibiting LD formation. These findings suggest that the effects of DOP may have potential clinical relevance.

Wnt signaling has been reported to inhibit adipogenic differentiation[52]. In this study, we found that HFD activated the expression of Wnt signaling-related genes, while DOP supplementation significantly enhanced the expression of these genes, leading to a marked upregulation of Wnt signaling. Consistently, we observed that DOP also inhibited the expression of genes related to lipid synthesis and adipogenesis, including *Fabp1*, *Fasn*, *Ldlr*, *Cebpb*, and *Dio2*. These findings suggest that DOP may suppress lipid synthesis and LD formation, thereby inhibiting adipocyte differentiation, possibly through the promotion of Wnt signaling.

Gut microbiota and its metabolites play a crucial role in regulating Wnt signaling[53]. Notably, DOP, as a type of acetylated glucomannan[54], may exert its physiological effects in a gut microbiota-dependent manner[55]. Consistently, we found that DOP reshaped the gut microbiota composition in DIO mice. HFD feeding caused the disappearance of over 300 microbial species, which were preserved in DIO mice treated with DOP. Furthermore, numerous microbes whose abundance was reversed by DOP intervention showed concordant associations with LD formation and the metabolic phenotypes of the mice. Using data-driven analysis, we identified two representative microbes, *B. pseudolongum* and *B. choerinum*, as potential mediators of DOP's regulatory effects on host metabolism. Previous studies have shown that *B. pseudolongum* can reduce body weight, visceral fat, and triglycerides in obese mice[56]. Similarly, reduced levels of *B. choerinum* have been linked to obesity, particularly in individuals with T2D[57]. These findings highlight the potential of DOP to modulate host metabolism through its effects on gut microbiota.

To model the signal transduction following DOP treatment from a systems biology perspective, we constructed a covariance network integrating the influence of DOP on the microbiome, metabolome, transcriptome, and phenotypic outcomes. Interrogating the network revealed the mechanistic pathways of DOP's regulatory effects, clearly demonstrating that DOP modulates gut microbiota and their metabolites, which, in turn, influence gene expression in adipose tissue, ultimately altering obesity-related phenotypic traits.

This study, employing multi-omics analytical tools, is the first to investigate the potential mechanisms by which DOP prevents DIO possibly through the Wnt signaling pathway and LD expansion. Substantial evidence indicates that DOP inhibits the deposition of dietary lipids in adipose tissue, suppresses endogenous lipid synthesis, and attenuates adipocyte maturation and hypertrophy. The overexpression of perilipins, which restricts the access of lipolytic enzymes to LDs, contributes to excessive LD expansion, making them promising therapeutic targets for obesity management. These findings suggest that DOP holds significant promise as a functional health food for obesity intervention.

The limitations of this study should be acknowledged as well. First, although our data suggest that DOP exerts its effects via the Wnt signaling pathway and perilipin-mediated regulation of lipid droplets, we did not directly manipulate these pathways or proteins. Further studies using genetic knockout models or specific inhibitors that target key components of these pathways or proteins are needed to conclusively establish the mechanisms underlying DOP’s anti-obesity effects. Furthermore, the specific microbes and

associated metabolites that may mediate the regulatory effects of DOP on adipose tissue require further elucidation. Lastly, it should also be recognized that the regulatory effects of DOP on other organs may contribute to its anti-obesity effects, and this aspect also warrants further investigation.

5. Conclusion

In summary, our integrated multi-omics analyses suggest that DOP may help alleviate diet-induced obesity in mice, potentially by modulating the gut microbiota and its metabolites, which could activate the Wnt signaling pathway in white adipose tissue. This modulation may contribute to the inhibition of lipid synthesis, reduction of lipid droplet formation, and improvement of metabolic dysfunction. These findings provide new insights into the possible mechanisms of DOP and highlight its potential as a functional food ingredient for the prevention and management of obesity and related metabolic disorders.

Disclosure statement

The authors have no conflicts of interest to declare.

Acknowledgements

We acknowledge the financial support provided by the Key Research and Development Project of Jiangxi Province (20224BBF62002), Jiangxi Provincial Natural Science Foundation (20242BAB20323, 20252BAC240712), National Natural Science Foundation of China (32402112), State Key Laboratory of Food Science and Technology Project (SKLF-ZZA-202211), and General Program of Natural Science Foundation of Jiangxi Province (20224BAB205040).

Reference

[1] A. Islam, H. Sultana, M. Nazmul Hassan Refat, et al., The global burden of overweight-obesity and its association with economic status, benefiting from STEPs survey of WHO member states: A meta-analysis, Prev Med Rep. 46 (2024) 102882.

[2] B. Mitrovic, Z.M. Gluvic, M. Obradovic, et al., Non-alcoholic fatty liver disease, metabolic syndrome, and type 2 diabetes mellitus: where do we stand today?, Archives of medical science: AMS. 19 (2022) 884.

[3] C.-H. Lai, C.-Y. Huo, J. Xu, et al., Critical review on the research of chemical structure, bioactivities, and mechanism of actions of Dendrobium officinale polysaccharide, International Journal of Biological Macromolecules. (2024) 130315.

[4] X. Chen, C. Chen, C. Ma, et al., Dendrobium officinale polysaccharide attenuates type 2 diabetes in mice model by modulating gut microbiota and alleviating intestinal mucosal barrier damage, Food Science and Human Wellness. (2024),

[5] Z. Li, Q. Nie, S.-P. Nie, Comprehensive insights: unraveling the mechanisms of gut commensals in glucose metabolism regulation, Science China. Life sciences. 67 (2024) 414-417.

[6] M. Gurung, Z. Li, H. You, et al., Role of gut microbiota in type 2 diabetes pathophysiology, EBioMedicine. 51 (2020),

[7] Z. Li, L. Chen, M. Sepulveda, et al., Microbiota-dependent and-independent effects of obesity on transplant rejection and hyperglycemia, American Journal of Transplantation. 23 (2023) 1526-1535.

[8] Z. Li, M. Gurung, R.R. Rodrigues, et al., Microbiota and adipocyte mitochondrial damage in type 2 diabetes are linked by Mmp12+ macrophages, Journal of Experimental Medicine. 219 (2022) e20220017.

[9] J. Fu, Y. Zheng, Y. Gao, et al., Dietary fiber intake and gut microbiota in human health, Microorganisms. 10 (2022) 2507.

[10] Z. Li, M. Gurung, R.R. Rodrigues, et al., Microbiota and adipocyte mitochondrial damage in type 2 diabetes are linked by Mmp12+ macrophages, J Exp Med. 219 (2022),

[11] M.A. Welte, A.P. Gould, Lipid droplet functions beyond energy storage, Biochimica et Biophysica Acta (BBA)-Molecular and Cell Biology of Lipids. 1862 (2017) 1260-1272.

[12] C. Sztalryd, D.L. Brasaemle, The perilipin family of lipid droplet proteins: Gatekeepers of intracellular lipolysis, Biochimica et biophysica acta (bba)-molecular and cell biology of lipids. 1862 (2017) 1221-1232.

[13] M. Imamura, T. Inoguchi, S. Ikuyama, et al., ADRP stimulates lipid accumulation and lipid droplet formation in murine fibroblasts, American Journal of Physiology-Endocrinology and Metabolism. 283 (2002) E775-E783.

[14] J. Gao, G. Serrero, Adipose differentiation related protein (ADRP) expressed in transfected COS-7 cells selectively stimulates long chain fatty acid uptake, Journal of Biological Chemistry. 274 (1999) 16825-16830.

[15] H. Itabe, T. Yamaguchi, S. Nimura, et al., Perilipins: a diversity of intracellular lipid droplet proteins, Lipids in health and disease. 16 (2017) 1-11.

[16] F. Sentinelli, D. Capoccia, M. Incani, et al., The perilipin 2 (PLIN2) gene Ser251Pro missense mutation is associated with reduced insulin secretion and increased insulin sensitivity in Italian obese subjects, Diabetes/metabolism research and reviews. 32 (2016) 550-556.

[17] P. Chandrasekaran, S. Weiskirchen, R. Weiskirchen, Perilipins: A family of five fat-droplet storing proteins that play a significant role in fat homeostasis, Journal of Cellular Biochemistry. 125 (2024) e30579.

[18] C. Sztalryd, M. Bell, X. Lu, et al., Functional compensation for adipose differentiation-related protein (ADFP) by Tip47 in an ADFP null embryonic cell line, Journal of Biological Chemistry. 281 (2006) 34341-34348.

[19] I. Buers, H. Robenek, S. Lorkowski, et al., TIP47, a lipid cargo protein involved in macrophage triglyceride metabolism, Arteriosclerosis, thrombosis, and vascular biology. 29 (2009) 767-773.

[20] W. Jiang, J. Tan, J. Zhang, et al., Polysaccharides from Dendrobium officinale improve obesity-induced insulin resistance through the gut microbiota and the SOCS3-mediated insulin receptor substrate-1 signaling pathway, Journal of the Science of Food and Agriculture. 104 (2024) 3437-3447.

[21] S. Yang, X. Huang, X. Li, et al., Aloe vera polysaccharides mitigate high-fat high-cholesterol diet-induced atherosclerosis in ApoE−/− mice via regulation of lipid metabolism and gut microbiota, Food & Function. 16 (2025) 6671-6686.

[22] X.-D. Shi, J.-Y. Yin, S.W. Cui, et al., Plant-derived glucomannans: Sources, preparation methods, structural features, and biological properties, Trends in Food Science & Technology. 99 (2020) 101-116.

[23] Y. Sun, Q. Nie, S. Zhang, et al., Parabacteroides distasonis ameliorates insulin resistance via activation of intestinal GPR109a, Nature Communications. 14 (2023) 7740.

[24] Z. Liao, J. Zhou, J. Lin, et al., Supplementation of Akkermansia muciniphila improves diabetic kidney disease by regulating gut microbiome in db/db mice, Food Bioscience. (2025) 107042.

[25] Z. Cao, H. Liu, P. Chen, et al., Integrative Evidence From Metabolome-Wide Mendelian Randomization and Animal Models Implicates Tyrosine in Cardiac Hypercontractility and Arrhythmia Risk, Food Frontiers. (2025),

[26] N.K. Newman, M.S. Macovsky, R.R. Rodrigues, et al., Transkingdom Network Analysis (TkNA): a systems framework for inferring causal factors underlying host-microbiota and other multi-omic interactions, Nat Protoc. 19 (2024) 1750-1778. https://doi.org/10.1038/s41596-024-00960-w.

[27] R.R. Rodrigues, M. Gurung, Z. Li, et al., Transkingdom interactions between Lactobacilli and hepatic mitochondria attenuate western diet-induced diabetes, Nature communications. 12 (2021) 101.

[28] P.J. Scarpace, Y. Zhang, Leptin resistance: a prediposing factor for diet-induced obesity, Am J Physiol Regul Integr Comp Physiol. 296 (2009) R493-500.

[29] M. Furuhashi, G.S. Hotamisligil, Fatty acid-binding proteins: role in metabolic diseases and potential as drug targets, Nat Rev Drug Discov. 7 (2008) 489-503.

[30] A.N. Günenc, B. Graf, H. Stark, et al., Fatty acid synthase: structure, function, and regulation, Macromolecular protein complexes iv: Structure and function. (2022) 1-33.

[31] M. Faraj, LDL, LDL receptors, and PCSK9 as modulators of the risk for type 2 diabetes: a focus on white adipose tissue, J Biomed Res. 34 (2020) 251-259.

[32] L. Guo, X. Li, Q.Q. Tang, Transcriptional regulation of adipocyte differentiation: a central role for CCAAT/enhancer-binding protein (C/EBP) β, J Biol Chem. 290 (2015) 755-761.

[33] E.H. Jho, T. Zhang, C. Domon, et al., Wnt/beta-catenin/Tcf signaling induces the transcription of Axin2, a negative regulator of the signaling pathway, Mol Cell Biol. 22 (2002) 1172-1183.

[34] Q. Tong, J. Tsai, G.S. Hotamisligil, GATA transcription factors and fat cell formation, Drug News Perspect. 16 (2003) 585-588. https://doi.org/10.1358/dnp.2003.16.9.829340.

[35] C. Christodoulides, C. Lagathu, J.K. Sethi, et al., Adipogenesis and WNT signalling, Trends in Endocrinology & Metabolism. 20 (2009) 16-24.

[36] Z. Li, H. Liu, Microbe-dependent and independent effects of diet on metabolic inflammation in glucose metabolism regulation, Food Chem. 488 (2025) 144852. https://doi.org/10.1016/j.foodchem.2025.144852.

[37] S.J. Mihalik, B.H. Goodpaster, D.E. Kelley, et al., Increased levels of plasma acylcarnitines in obesity and type 2 diabetes and identification of a marker of glucolipotoxicity, Obesity (Silver Spring). 18 (2010) 1695-1700.

[38] V. Gopalan, N. Michael, S. Ishino, et al., Effect of Exercise and Calorie Restriction on Tissue Acylcarnitines, Tissue Desaturase Indices, and Fat Accumulation in Diet-Induced Obese Rats, Sci Rep. 6 (2016) 26445.

[39] X. Chen, C. Chen, C. Ma, et al., Dendrobium officinale polysaccharide attenuates type 2 diabetes in mice model by modulating gut microbiota and alleviating intestinal mucosal barrier damage, Food Science and Human Wellness. 14 (2025),

[40] J. Fang, Y. Lin, H. Xie, et al., Dendrobium officinale leaf polysaccharides ameliorated hyperglycemia and promoted gut bacterial associated SCFAs to alleviate type 2 diabetes in adult mice, Food chemistry: X. 13 (2022) 100207.

[41] Y. Liu, L. Yang, Y. Zhang, et al., Dendrobium officinale polysaccharide ameliorates diabetic hepatic glucose metabolism via glucagon-mediated signaling pathways and modifying liver-glycogen structure, Journal of ethnopharmacology. 248 (2020) 112308.

[42] J. Qu, S. Tan, X. Xie, et al., Dendrobium Officinale Polysaccharide Attenuates Insulin Resistance and Abnormal Lipid Metabolism in Obese Mice, Frontiers in Pharmacology. 12 (2021) 1490.

[43] R.A. van der Heijden, F. Sheedfar, M.C. Morrison, et al., High-fat diet induced obesity primes inflammation in adipose tissue prior to liver in C57BL/6j mice, Aging (Albany NY). 7 (2015) 256-268.

[44] E.W. Kraegen, P.W. Clark, A.B. Jenkins, et al., Development of muscle insulin resistance after liver insulin resistance in high-fat-fed rats, Diabetes. 40 (1991) 1397-1403. https://doi.org/10.2337/diab.40.11.1397.

[45] M. Małodobra-Mazur, A. Cierzniak, D. Pawełka, et al., Metabolic Differences between Subcutaneous and Visceral Adipocytes Differentiated with an Excess of Saturated and Monounsaturated Fatty Acids, Genes (Basel). 11 (2020),

[46] J.A. Olzmann, P. Carvalho, Dynamics and functions of lipid droplets, Nature reviews Molecular cell biology. 20 (2019) 137-155.

[47] L.L. Listenberger, A.G. Ostermeyer-Fay, E.B. Goldberg, et al., Adipocyte differentiation-related protein reduces the lipid droplet association of adipose triglyceride lipase and slows triacylglycerol turnover, J Lipid Res. 48 (2007) 2751-2761. https://doi.org/10.1194/jlr.M700359-JLR200.

[48] S. Kaushik, A.M. Cuervo, AMPK-dependent phosphorylation of lipid droplet protein PLIN2 triggers its degradation by CMA, Autophagy. 12 (2016) 432-438.

[49] C.P. Najt, M. Devarajan, D.G. Mashek, Perilipins at a glance, J Cell Sci. 135 (2022),

[50] R.M. Carr, R.T. Patel, V. Rao, et al., Reduction of TIP47 improves hepatic steatosis and glucose homeostasis in mice, Am J Physiol Regul Integr Comp Physiol. 302 (2012) R996-1003.

[51] D. Ferguson, J. Zhang, M.A. Davis, et al., The lipid droplet-associated protein perilipin 3 facilitates hepatitis C virus-driven hepatic steatosis, J Lipid Res. 58 (2017) 420-432.

[52] N.K.H. Yiew, T.K. Chatterjee, Y.L. Tang, et al., A novel role for the Wnt inhibitor APCDD1 in adipocyte differentiation: Implications for diet-induced obesity, J Biol Chem. 292 (2017) 6312-6324.

[53] S.S. Kumar, A. Fathima, P. Srihari, et al., Host-gut microbiota derived secondary metabolite mediated regulation of Wnt/β-catenin pathway: a potential therapeutic axis in IBD and CRC, Front Oncol. 14 (2024) 1392565.

[54] X. Guo, M. Yang, C. Wang, et al., Acetyl-glucomannan from Dendrobium officinale: Structural modification and immunomodulatory activities, Frontiers in Nutrition. 9 (2022) 1016961.

[55] L. Xu, X. Zeng, Y. Liu, et al., Effect of Dendrobium officinale polysaccharides on central nervous system disease: Based on gut microbiota, International Journal of Biological Macromolecules. 240 (2023) 124440.

[56] T.B. Bo, J. Wen, Y.C. Zhao, et al., Bifidobacterium pseudolongum reduces triglycerides by modulating gut microbiota in mice fed high-fat food, J Steroid Biochem Mol Biol. 198 (2020) 105602. https://doi.org/10.1016/j.jsbmb.2020.105602.

[57] A.I. Suceveanu, A.P. Stoian, I. Parepa, et al., Gut microbiota patterns in obese and type 2 diabetes (T2D) patients from romanian black sea coast region, Rev Chim. 69 (2018) 2260-2267.